A Brownian Dynamics Algorithm for Arbitrary Rigid Bodies. Application to Polarized Dynamic Light Scattering

Stuart A. Allison

Department of Chemistry, Georgia State University, Atlanta, Georgia 30329

Received May 10, 1990; Revised Manuscript Received July 13, 1990

ABSTRACT: A Brownian dynamics algorithm is developed to simulate dynamics experiments of rigid macromolecules. It is applied to polarized dynamic light scattering from rodlike structures and from a model of a DNA fragment (762 base pairs). A number of rod cases are examined in which the translational anisotropy is increased from zero to a large value. Simulated first cumulants as well as amplitudes and lifetimes of the dynamic form factor are compared with predictions of analytic theories and found to be in very good agreement with them. For DNA fragments 762 base pairs in length or longer, translational anisotropy does not contribute significantly to dynamic light scattering. In a comparison of rigid and flexible simulations on semistiff models of this fragment, it is shown directly that flexing contributes to the faster decay processes probed by light scattering and that the flexible model studies are in good agreement with experiment.

I. Introduction

Relaxation methods like fluorescence depolarization, birefringence, and dynamic light scattering have been very useful in studying the conformation and dynamics of macromolecules. With regards to rigid model macromolecules in general, analytic theories have been successful in predicting fluorescence depolarization[1,2] and electric birefringence[3] experiments. In these cases, the experiments are sensitive to only rotational motions. The interpretation of dynamic light scattering is more difficult since this technique is sensitive to both translational and rotational motions. Aragon and Pecora[4] have developed a theory of dynamic light scattering from a dilute solution of arbitrary rigid macromolecules assuming translational and rotational motions are uncoupled. However, for very anisotropic bodies like long rods, which serve as simple but reasonable models for such structures as filamentous viruses,[5] F-actin,[6] and muscle filament,[7] the translational and rotational motions are coupled. (The translational diffusion constant is different parallel and perpendicular to the long axis of the rod, and the orientation of the long axis changes as the rod rotates.) The effect of this coupling on dynamic light scattering from dilute solutions of rodlike molecules has been studied by a number of investigators.[8-14] Recently, Aragon and Pecora[15] have formulated a comprehensive analytic theory that is valid for any rigid body provided it possesses cylindrical symmetry. The general case of an arbitrary rigid body without cylindrical symmetry and with translation-rotation coupling remains unsolved.

In this work, a Brownian dynamics algorithm is developed in which relaxation experiments can be simulated for general models of rigid macromolecules. The algorithm is described in section II with details placed in the Appendix. It is applied to polarized dynamic light scattering from an array of subunits treated as point scatterers in the usual Rayleigh-Debye approximation. Dynamic light-scattering correlation functions are analyzed by the method of cumulants[16] and by CONTIN,[17] which estimates the distribution of relaxation times that comprise the correlation function. Other techniques (fluorescence depolarization, depolarized light scattering, and electric birefringence) are more sensitive to the rotational motions of macromolecules. However, analytic theories for rigid molecules are currently available for these techniques, which render simulations unnecessary unless one is only interested in verifying the simulation algorithm. Results are presented and discussed in section III. To test the algorithm, simulations are first carried out on rods modeled as three identical equally spaced subunits with varying degrees of translation-rotation coupling. The simulation results are compared in a quantitative way with analytic theory, and agreement is found to be excellent. If the difference between the translational diffusion constants parallel and perpendicular to the symmetry axis are not large, then translation-rotation coupling has little effect on the first cumulant or the distribution of relaxation times. Although translation-rotation coupling may be important in the case of a highly asymmetric structure like the tobacco mosaic virus,[5,11,14] it is not very important in a less asymmetric (but hardly spherical) structure like a 762 base pair DNA fragment.[18] We end by comparing simulated dynamic light-scattering results of rigid and flexible 10-subunit models of a 762 base pair DNA fragment with actual experiments.[18] This comparison illustrates that segmental flexibility has a significant effect on the faster relaxation time present (the first internal time). The first internal time is consistently longer for rigid structures compared to flexible structures. The main conclusions of this work are summarized in section IV.

II. Methods

The basic strategy followed here regarding rigid bodies is similar to previous Brownian dynamics simulations of flexible structures.[19,20] A structure is first generated and its dynamical evolution is followed for a certain length of time. This constitutes a trajectory during which single trajectory correlation functions relevant to certain relaxation experiments (fluorescence depolarization, electric birefringence, and dynamic light scattering) are calculated and averaged. This procedure is repeated on a large number of trajectories, and ensemble-averaged correlation functions are determined.

The convention of representing vector quantities with bold lower case and tensor quantities with bold upper case characters will generally be followed. Eigenvalue matrices of the diffusion tensors shall be represented with a boldface λ. Let $\mathbf{D}_r(t_0)$, $\mathbf{D}_t(t_0)$, and $\mathbf{r}_{CD}(t_0)$ denote the configuration-dependent rotational and translational diffusion tensors and center of diffusion, respectively, of an arbitrary structure at some initial time t_0 in some convenient laboratory frame of reference. For simple geometries like rods and symmetric ellipsoids, it is straightforward to determine $\mathbf{D}_r(t_0)$ and $\mathbf{D}_t(t_0)$ by using analytic expressions.[21] For complex objects modeled as rigid bead arrays, there are a number of algorithms available that can be used to determine these quantities.[21-23] We find the algorithm of Garcia de la Torre and

0024-9297/91/2224-0530$02.50/0

co-workers[23] particularly convenient. Subroutines EIGRS or EVCSF of the IMSL subroutine library[24] can then be used to determine the eigenvalues and eigenvectors of $\mathbf{D}_r(t_0)$ and $\mathbf{D}_t(t_0)$. For brevity sake, the r and t subscripts as well as the time dependence is suppressed below. The diagonal eigenvalue matrix and normalized orthogonal column eigenvectors of $\mathbf{D}$, $\mathbf{z}_i$ (i = 1 and 3) are related by

$$\lambda = \mathbf{Z}^T\mathbf{D}\mathbf{Z} \tag{1}$$

where the T superscript denotes transpose and $\mathbf{Z}$ the 3×3 unitary matrix

$$\mathbf{Z} = [(\mathbf{z}_1)(\mathbf{z}_2)(\mathbf{z}_3)] \tag{2}$$

As discussed at the beginning of the Appendix, we can identify

$$\mathbf{Q} = \mathbf{K}\mathbf{Z}^T \tag{3}$$

where $\mathbf{Q}$ is the Cartesian rotation matrix, which transforms the lab frame into the principal axis (pa) frame, and $\mathbf{K}$ is a simple diagonal matrix given by eq A2. As shown in the Appendix, $\mathbf{K}$ has no effect on the average dynamical evolution of the structure so the eigenvector matrix, $\mathbf{Z}$, can be equated to the transpose of the rotation matrix $\mathbf{Q}^T$.

At the start of a trajectory, the subunit coordinates, $\mathbf{r}_i(t_0)$, are known as well as $\mathbf{r}_{CD}(t_0)$, λ_r, λ_t, $\mathbf{Z}_r(t_0)$, and $\mathbf{Z}_t(t_0)$. Also important are subunit coordinates relative to the center of diffusion defined by

$$\mathbf{s}_i(t) = \mathbf{r}_i(t) - \mathbf{r}_{CD}(t) \tag{4}$$

During dynamics, the structure rotates and translates. In this work, the strategy is to follow the time evolution of the $\mathbf{Q}$ matrices, which transform the lab frame into the instantaneous pa frames of translation (pat) and rotation (par). In these reference frames, translational and rotational displacements are independent about orthogonal axes and can be generated by using Gaussian random numbers. This is valid provided the orientation of the structure does not change significantly during the dynamics time step, δt. To avoid a lengthy digression, the details of this strategy are relegated to the Appendix, and only final results are presented here. Rotational motion determines the time evolution of $\mathbf{s}_i$. After the nth dynamics step

$$\mathbf{s}_i(t_n) = \mathbf{Z}_r(t_0)\,\mathbf{P}(t_0,t_n)\,\mathbf{Z}_r^T(t_0)\,\mathbf{s}_i(t_0) \tag{5}$$

where $t_n = t_0 + n\delta t$

$$\mathbf{P}(t_0,t_n) = \mathbf{U}^T(t_0,\delta t)\,\mathbf{U}^T(t_1,\delta t)\ldots\mathbf{U}^T(t_{n-1},\delta t) \tag{6}$$

and the $\mathbf{U}$ matrices are defined by eqs A8 and A9. Each of the $\mathbf{U}$ matrices represents the rotation of the structure in the par frame during a particular dynamics step. The $\mathbf{P}$ matrix is constantly updated during a trajectory. For dynamics step $n + 1$

$$\mathbf{P}(t_0,t_{n+1}) = \mathbf{P}(t_0,t_n)\mathbf{U}^T(t_n,\delta t) \tag{7}$$

Rotational and translational motions enter in the time evolution of the center of diffusion

$$\mathbf{r}_{CD}(t_{n+1}) = \mathbf{r}_{CD}(t_n) + \delta\mathbf{r}_{CD}(t_n) \tag{8}$$

$$\delta r_{CD}(t_n) = \mathbf{Z}_r(t_0)\,\mathbf{P}(t_0,t_n)\,\mathbf{Z}_r^T(t_0)\,\mathbf{Z}_t(t_0)\,\lambda_t^{1/2}\mathbf{x}_{CD} \tag{9}$$

where $\lambda_t^{1/2}$ is a diagonal matrix with elements equal to the square root of the elements of λ_t and $\mathbf{x}_{CD}$ is a vector of independent Gaussian random numbers of 0 mean and variance $(2\delta t)^{1/2}$. In some simulations, translational diffusion is suppressed, which means that eqs 8 and 9 are bypassed during dynamics. In these cares, the only motion the structures undergo is rotation about the center of diffusion (eq 5).

To simulate a particular experiment, an appropriate average must be computed. In the case of polarized dynamic light scattering, it is the dynamic scattering form factor[25]

$$S(q,t) = N^{-2}\langle\sum_{i=1}^{N}\sum_{j=1}^{N}\exp[-i\mathbf{q}\cdot(\mathbf{r}_i(t') - \mathbf{r}_j(t'+t))]\rangle \tag{10}$$

where N is the number of scattering elements, $\mathbf{q}$ is the scattering vector of magnitude

$$q = (4\pi n/\lambda)\sin(\theta/2) \tag{11}$$

n is the refractive index (set to 1.3334), λ is the wavelength of scattered light, and θ is the scattering angle.

The dynamic form factors are then analyzed by CONTIN, a model independent data analysis program developed by Provencher and co-workers.[17] Analysis by CONTIN yields the distribution of relaxation times, $G(q,\tau)$, which is related to the form factor by

$$S(q,t) = \int_0^\infty G(q,\tau)\exp(-t/\tau)\,d\tau \tag{12}$$

In general, determination of $G(q,\tau)$ is an ill-posed problem since many possible solutions exist that fit the data within experimental error. CONTIN formulates the problem in terms of a weighted least-squares fit with an added quadratic term, the regularizor, which imposes smoothness on the solution. For the applications considered here, $S(q,t)$ consists of a single decay process at low q^2 ($q^2 < 10^{10}$ cm^2) due to overall translational diffusion. As q^2 is increased, an additional decay process appears, which, for rigid structures, corresponds to coupled translational and rotational diffusion.[4,15,18,26] The amplitude of this additional decay process increases with scattering vector but remains small relative to that due to translational diffusion for $q^2 < 10^{11}$ cm^{-2} and for particle sizes whose overall linear dimensions are less than about 1800 Å. For q^2 greater than 10^{11} cm^{-2}, additional decays begin to contribute significantly to $S(q,t)$, but this lies outside the range readily accessible in most experimetal light-scattering studies and this scattering vector range will not be considered here. In this work then, $S(q,t)$ generally consists of a large-amplitude slow decay and a small-amplitude fast decay. Under these circumstances, it has been our experience that there is considerable uncertainty in the amplitude and lifetime of the faster peak when simulation data is analyzed by CONTIN.[20] To determine how large this uncertainty is, three independent simulations are carried out for each of the case studies reported. Each simulation is analyzed separately by CONTIN as well as the data set obtained by averaging the $S(q,t)$'s from all three. From this analysis, the standard deviations in peak lifetimes and amplitudes can be estimated. Here, a single simulation consists of 300 trajectories and each trajectory lasts 0.020 s with δt = 500 ns (40 000 dynamics steps). The first 61 time points of $S(q,t)$ are calculated with a time resolution of 2 μs and the remaining points with a time resolution of 20 μs. In simulations with translational diffusion suppressed, reproducibility is greatly improved and only 100–250 trajectories per simulation are carried out in those cases. The analysis protocol is otherwise identical with that described above.

In additional to peak amplitudes and lifetimes, the first cumulant, K_1, shall also be determined. It can be written[20] as

$$K_1 = \int_0^\infty \tau^{-1}\,G(q,\tau)\,d\tau/S(q,0) \tag{13}$$

where terms have the same meaning as in eq 12. First cumulants can be obtained from the CONTIN output since the moment, $\langle\tau^{-1}\rangle$, is tabulated. Values of K_1 reported here are obtained in this way. Occasionally, anomalously large values of K_1 are observed in certain simulations, which can be traced to a spurious small-amplitude decay component of $G(q,\tau)$ at very short τ (typically 1–5 μs where no component is expected). This phenomenon has been reported previously.[20] Another diagnostic feature is a large variation in $\langle\tau^{-1}\rangle$ as the contribution of the regularizor in the CONTIN weighted lease-squares analysis is varied. Because multiple simulations are reported here, we can discard such cases when they are easily identified. Nonetheless, this effect or at least mild cases thereof is probably responsible for the uncertainty in K_1 reported here and their tendency to be larger than expected.

Table I
Comparison of Theoretical and Simulated (Translational Diffusion Suppressed) Amplitudes and Lifetimes[a]

q^2, in 10^{10} cm^{-2}	theory			simulation		
	a_0	a_1	a_2	a_1[b]	a_2	τ_1,[b] 10^{-6} s
2.684	0.704	0.019		0.020		92
4.171	0.580	0.041		0.042 (0.001)		94 (3)
4.871	0.531	0.053		0.054		91
5.895	0.466	0.071		0.074 (0.002)		96 (2)
7.520	0.370	0.100	0.001	0.103		94
9.105	0.299	0.126	0.002	0.130 (0.002)		92 (2)
11.79	0.210	0.165	0.005	0.169		89

[a] From theory, $\tau_1 = 1/6\Theta = 90$ μs. [b] Quantities in parentheses denote standard deviations.

III. Results and Discussion

As a first application of the algorithm, we consider a rod made up of three subunits with an intersubunit separation (b) of 765 Å, translational diffusion constants parallel ($D_\parallel$) and perpendicular ($D_\perp$) to the rod axis of 0.909×10^{-7}cm^2/s, and a rotational diffusion constant perpendicular to the rod axis (Θ) of 0.185×10^4 s^{-1}. Rotational diffusion about the rod axis does not contribute to dynamic light scattering and is left out. These transport coefficients correspond closely to those expected for a "trumbell" rod with $b = 765$ Å and subunit radii of 94.6 Å when the Rotne–Prager tensor[27] is used to calculate the hydrodynamic interaction between the subunits. A trumbell refers to a rigid or flexible linear chain made up of three identical subunits and connected to each other by two identical virtual bonds. In each case of a trumbell rod, the subunits are collinear. For such a structure, it can be shown that $D_\parallel = 0.985 \times 10^{-7}$ cm^2/s, $D_\perp = 0.871 \times 10^{-5}$ cm^2/s, and $\Theta = 0.185 \times 10^4$ s^{-1}. The orientationally averaged translational diffusion constant

$$D = (D_\parallel + 2D_\perp)/3 \tag{14}$$

equals 0.909×10^{-7} cm^2/s. In an actual trumbell rod, translational diffusion constants parallel and perpendicular to the rod axis are not identical. In the first case study, this translational anisotropy is ignored and D is used to approximate $D_\parallel$ and $D_\perp$.

It should be possible to compare simulation results in this case with the theory of Pecora[25,28] for a translationally isotropic rod of N subunits. This theory predicts

$$S(q,t) = \exp(-q^2Dt)\sum_{k=0}^{\infty} a_k(q)\exp[-2k(2k+1)\Theta t] \tag{15}$$

where

$$a_k(q) = 4N^{-2}(4k+1)[\sum_{m=1}^{N/2} j_{2k}((2m-1)qb/2)]^2 \tag{16}$$

for even N

$$a_k(q) = N^{-2}[\delta_{k0} + 2(4k+1)^{1/2}\sum_{m=1}^{(n-1)/2} j_{2k}(mqb)]^2 \tag{17}$$

for odd N, δ_{k0} is the Kronecker delta, and j_{2k} is a spherical Bessel function of order $2k$. The first cumulant is given by

$$K_1 = \sum_{k=0}^{\infty}(q^2D + 2k(2k+1)\Theta)a_k(q)/\sum_{k=0}^{\infty} a_k(q) \tag{18}$$

In order to simplify the simulated decays as much as possible, translational diffusion is first suppressed (hereafter referred to as TDS simulations). Table I summarizes the comparison of theoretical and simulated ($a_0 = 0$) amplitudes and lifetimes. Agreement is seen to be very good, with a high degree of reproducibility between different simulations. Although this confirms the soundness of the algorithm, it does not constitute a very stringent test of CONTIN since the decay consists essentially of a single-exponent decay. $G(q,\tau)$ at three q^2 obtained from the simulation are shown in Figure 1.

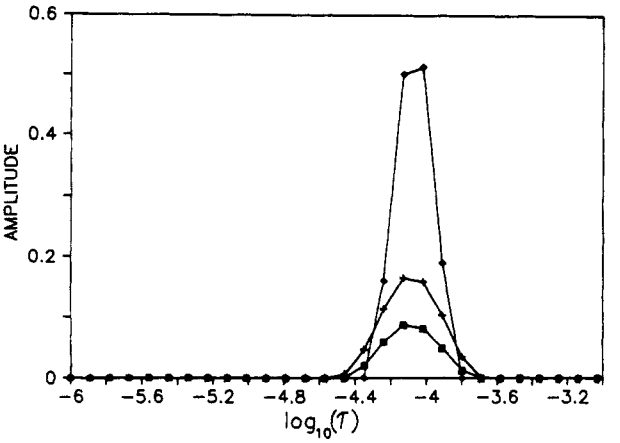

Figure 1. $G(q,\tau)$ for an isotropic rod (translation suppressed). Squares, crosses, and diamonds correspond to $q^2 = 4.171$, 5.895, and 9.105×10^{10} cm^{-2}, respectively. Amplitude is in arbitrary units.

Inclusion of translational diffusion is carried out in two ways. In case 1, the dynamic form factors obtained from the TDS simulations described above are simply multiplied by $\exp(-q^2Dt)$ prior to CONTIN analysis. In case 2, translational diffusion is carried out explicitly. Since the translational diffusion tensor is taken to be isotropic in case 2, both should be indistinguishable. On the basis of Table II, which summarizes the CONTIN peak amplitudes and lifetimes, this is evidently the case. Figure 2 shows an example of $G(q,\tau)$ for three independent simulations. The standard deviations listed in Table II are derived from the variation in peak amplitudes and positions. When the amplitudes of Tables I and II are compared, lower values of a_1 are consistently obtained when the full decay is analyzed. The lifetimes also come out lower. Correcting the faster lifetimes, τ, for the contribution of translation ($\tau' = \tau/(1 - q^2D\tau)$) yields $\tau' = 70 \pm 5$ (case 1) and 72 ± 6 μs (case 2) for $4.171 \times 10^{10} \le q^2 \le 7.52 \times 10^{10}$ cm^{-2}. The theoretical value is 90 μs. As discussed by Sorlie and Pecora in connection with CONTIN fits to form factors of Rouse models,[26] one should not *directly* equate amplitudes and lifetimes from analytic theories, which predict a superposition of two or more discrete decays with the corresponding quantities extracted from a CONTIN analysis. This is because CONTIN tends to fit the data to a fairly broad distribution and, under certain conditions, separate resolved peaks farther apart than it should (peak "repulsion"). This effect is due, in large part at least, to a small

Table II
Peak Amplitudes and Lifetimes for Translationally Isotropic Rods[a]

	case 1[b]		case 2[c]	
q^2, 10^{10} cm^{-2}	a	τ, 10^{-6} s	a	τ, 10^{-6} s
2.684	0.012	47	0.009 (0.002)	33 (9)
	0.711	407	0.714 (0.001)	405 (1)
4.171	0.034 (0.007)	58 (8)	0.025 (0.005)	56 (6)
	0.587 (0.007)	261 (2)	0.594 (0.009)	259 (2)
4.871	0.036	50	0.042 (0.006)	60 (7)
	0.548	221	0.542 (0.009)	222 (2)
5.895	0.042 (0.006)	49 (4)	0.035 (0.010)	47 (3)
	0.495 (0.010)	180 (3)	0.502 (0.009)	178 (2)
7.52	0.066 (0.009)	48 (3)	0.058 (0.014)	48 (5)
	0.405 (0.010)	140 (2)	0.413 (0.009)	138 (2)
9.105[d]	0.107 (0.026)	50 (8)	0.007 (0.010)	45 (4)
	0.320 (0.030)	115 (5)	0.349 (0.009)	112 (2)
11.79	0.380	71	0.380 (0.001)	72 (2)

[a] Quantities in parentheses denote standard deviations. [b] Center of diffusion subtracted out during dynamics. Translational diffusion accounted for by multiplying $S(q,t)$ by $\exp(-q^2Dt)$. [c] Center of diffusion not subtracted out during dynamics. [d] At this q^2, the two peaks are merged in certain simulations. Listed values are from simulations where they are resolved.

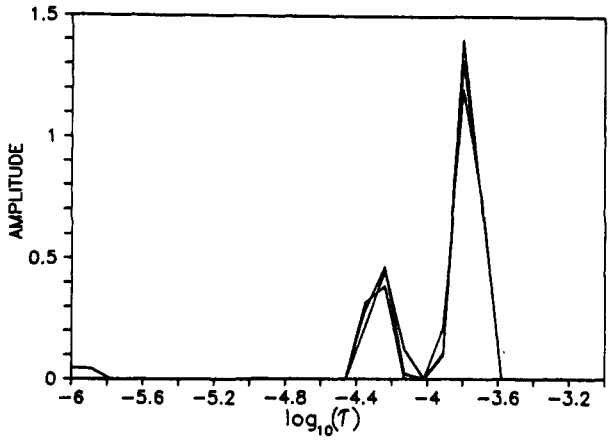

Figure 2. $G(q,\tau)$ for three independent simulations (translational diffusion included). The case is for the isotropic rod described in the text at $q^2 = 5.895 \times 10^{10}$ cm^{-2}. The longtime peak represents overall translation and the faster peak the coupled rotation–translation mode. Amplitude is in arbitrary units.

level of noise in experimental or simulated data. To illustrate this, consider an example of a biexponential decay with amplitudes a_0 and a_1 of 0.580 and 0.041 and lifetimes τ_0 and τ_1 of 264 and 67 μs, which corresponds to $q^2 = 4.171 \times 10^{10}$ cm^{-2}. If CONTIN is used to fit a pure decay, the amplitudes and decays are accurately reproduced. If, however, Gaussian random noise with a standard deviation of 0.001 (comparable to the noise level in the simulations) is superimposed on the decay, then a_0 and $a_1 = 0.593$ and 0.029 and τ_0 and $\tau_1 = 260$ and 56. When these amplitudes and lifetimes are compared with the $q^2 = 4.171 \times 10^{10}$ cm^{-2} values listed in Table II, it can be seen that this noise "correction" brings theory and simulation into excellent agreement.

Attention shall now be turned to the effect of anisotropic translational diffusion on dynamic light scattering, which is ignored in the Pecora model. Wilcoxon and Schurr[11] have derived analytic equations for the first cumulant of a rod of equally spaced beads of separation b, which is translationally anisotropic. They find

$$K_1/q^2 = D_\parallel - (D_\parallel - D_\perp)g_1(q) + \Theta b^2 g_2(q) \qquad (19)$$

where g_1 and g_2 represent spatial averages over the scattering elements of the rod, and simple analytic

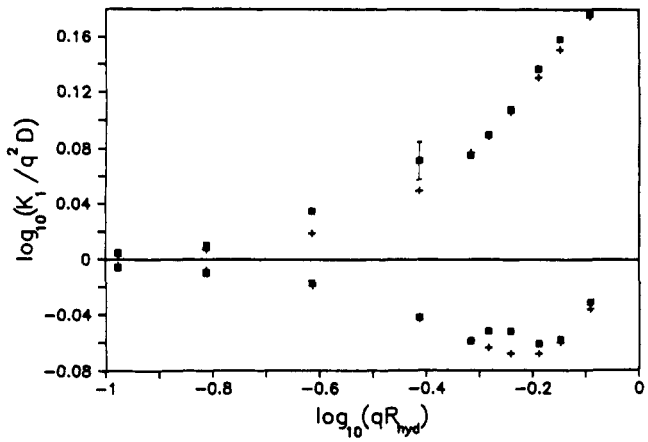

Figure 3. First cumulants of three subunit rods. Crosses/squares denote theory/simulation with the upper pair of points corresponding to an isotropic rod ($D_\parallel = D_\perp = 0.909 \times 10^{-7}$ cm^2/s) and the lower set of points corresponding to a highly anisotropic rod ($D_\parallel = 2.327 \times 10^{-7}$ and $D_\perp = 0.20 \times 10^{-7}$ cm^2/s). The error bar denotes approximate uncertainties in the simulations. Also, $R_{hyd} = k_BT/6\pi\eta D$.

expressions for them can be found in the above reference. Maeda and Fujime have derived a similar relation for K_1 for a continuum rod model as well as expressions (left in the form of integral equations) for the dynamic form factor.[13] Plotted in Figure 3 are theoretical and simulated first cumulants for two extreme cases of translational anisotropy. Theoretical/simulated cumulants are denoted by crosses/squares with the upper two sets of points corresponding to the isotropic case ($D_\parallel = D_\perp = 0.909 \times 10^{-7}$ cm^2/s) and the lower two sets of points corresponding to a highly anisotropic case ($D_\perp = 0.20$ cm^2/s, $D_\parallel = 2.327 \times 10^{-7}$ cm^2/s). It is clear from this figure that the first cumulant is sensitive to translational anisotropy when the difference between $D_\parallel$ and $D_\perp$ is large. Actual lifetimes and amplitudes obtained from simulations (from CONTIN first moments) along with lifetimes and amplitudes predicted by the theory of Aragon and Pecora[15] are summarized in Table III for a variety of cases at two different scattering vectors. As in the isotropic case discussed previously, a_1 and τ_1 from simulations are consistently smaller than those in the theoretical predictions, and this is due to noise. Perhaps it is worthwhile to briefly discuss the effect translational anisotropy has on amplitudes and lifetimes. For the faster component, increasing anisotropy produces a modest decrease in τ_1 but a large reduction in a_1. For the slow component, increasing anisotropy produces a modest increase in both a_0 and τ_0. Hence, the most significant effect is a reduction in a_1.

Whether or not translational anisotropy is important depends on the system of interest. For tobacco mosaic virus and certain long filamentous structures, it evidently cannot be ignored.[8-14] In the case of DNA fragments of length 2591 Å (762 base pairs), the effect is expected to be much smaller. DNA can be modeled as a wormlike chain with a persistence length of 500–1000 Å, depending on solvent conditions.[29] Summarized in Table IV are elements of the ensemble-averaged translational diffusion tensor in the pat frame (D_1, D_2, D_3) along with $D = (D_1 + D_2 + D_3)/3$ and the corresponding Kirkwood diffusion constant[21] for $P = 500$ and 1000 Å. These transport properties are obtained as follows. Following Hagerman and Zimm,[22] 100 chains of 82 subunits each are generated and "frozen" in their initial configurations for both cases. This number of beads reproduces the contour length of a 762 base pair DNA fragment. For each chain, the

Table III
Amplitude and Lifetimes of Anisotropic Rods Modeled as Three Beads[a]

case[b]	q^2, 10^{10} cm^{-2}	a_0	τ_0, 10^{-6} s	a_1	τ_1, 10^{-6} s
$D_\parallel = 0.909$	4.17	0.590 ± 0.005 (0.580)	260 ± 2 (264)	0.030 ± 0.006 (0.041)	57 ± 8 (67)
$D_\perp = 0.909$	7.52	0.409 ± 0.012 (0.370)	139 ± 3 (146)	0.061 ± 0.014 (0.100)	48 ± 3 (56)
$D_\perp = 0.800$	4.17	0.599 ± 0.007 (0.591)	263 ± 1 (265)	0.022 ± 0.004 (0.031)	58 ± 5 (66)
$D_\parallel = 1.127$	7.52	0.410 ± 0.008 (0.393)	144 ± 2 (147)	0.060 ± 0.011 (0.077)	50 ± 6 (54)
$D_\perp = 0.600$	4.17	0.614 ± 0.002 (0.605)	269 ± 1 (272)	0.008 ± 0.002 (0.017)	40 ± 8 (64)
$D_\parallel = 1.527$	7.52	0.441 ± 0.002 (0.424)	150 ± 1 (154)	0.028 ± 0.002 (0.046)	42 ± 3 (51)
$D_\perp = 0.200$	4.17	0.619 ± 0.001 (0.619)	307 ± 1 (307)	(0.003)	(59)
$D_\parallel = 2.327$	7.52	0.465 ± 0.002 (0.451)	185 ± 1 (196)	0.005 ± 0.002 (0.019)	21 ± 5 (46)

[a] Entries with standard deviations (±) represent simulations and those in parentheses are derived from Aragon–Pecora theory.[15] [b] All entries are in 10^{-7} cm^2/s.

Table IV
Translational Transport Properties for 762 Base Pair DNA[a]

	P = 500 Å[b]	P = 1000 Å[b]
D_1	0.784 (0.003)	0.723 (0.003)
D_2	0.854 (0.004)	0.784 (0.004)
D_3	0.982 (0.004)	0.969 (0.004)
D	0.873	0.825
$D_{Kirkwood}$	0.910	0.862
Δ[c]	0.187	0.261

[a] Standard deviations in parentheses. [b] All entries in 10^{-7} cm^2/s. [c] $\Delta \equiv (D_3 - (D_1 + D_2)/2)/D$.

translational diffusion tensor is determined and diagonalized[23] and the results are averaged over all chains. Although this case lacks cylindrical symmetry as evidenced by the difference in D_1 and D_2, we shall simply define a reduced anisotropy

$$\Delta = (D_3 - (D_1 + D_2)/2)/D \tag{20}$$

and compare it with the corresponding quantity for the cases in Table III in order to get a rough idea of the importance of translational anisotropy. For the actual DNA, $\Delta \approx 0.2$ whereas the rod with $D_\perp$ and $D_\parallel = 0.80$ and 1.127×10^{-7} cm^2/s has $\Delta = 0.36$. Consequently, we would not expect translational anisotropy to have a significant effect on the dynamic light scattering from 762 base pair DNA.

An obvious model for 762 base pair DNA is the 82 subunit Hagerman–Zimm model discussed above. Unfortunately, computing costs are prohibitive for chains of this size and simpler models have to be used. (CPU time varies as N^3 for calculating rigid-body transport coefficients and as N^2 for dynamic light-scattering simulations of rigid macromolecules.) Such models have been described in previous electric birefringence[30] and dynamic light-scattering[20] simulations of flexible DNA models. In the present work, 762 base pair DNA is modeled as a linear string of 10 beads with bead radius 39.7 Å and average virtual bond length of 255 Å. Stiffness is introduced via bending, g, and stretching, c, force constant parameters of 2 and 100, respectively. For a detailed description of the model, the reader is referred to ref 20. This model has essentially the same D and rms end-to-end distance as an 82 subunit Hagerman–Zimm chain with a persistence length of 500 Å and is expected to reproduce the dynamic structure factor of the more realistic model at low scattering vector ($q^2 < 10^{11}$ cm^{-2}). A key question we want to address is how chain flexibility influences a_1 and τ_1. Consequently, parallel simulations of rigid and flexible model chains are compared below. Methods used to carry out the flexible studies have been described previously.[20] Because translational anisotropy is small, the center of diffusion/center of mass coordinates are reset to the origin in rigid/flexible simulations. Dynamic structure factors determined from these TDS simulations can then be corrected to account

Table V
Comparison of Rigid and Flexible Model Studies of 762 Base Pair DNA (Translational Diffusion Suppressed)[a]

	rigid		flexible	
q^2, 10^{10} cm^{-2}	a	τ[b]	a	τ[b]
2.684	0.009 (0.001)	63 (12)	0.010 (0.001)	45 (10)
4.171	0.024 (0.001)	79 (5)	0.028 (0.002)	47 (5)
4.871	0.031 (0.002)	77 (5)	0.038 (0.002)	53 (6)
5.895	0.002 (0.001)	11 (4)	0.003 (0.002)	4 (2)
	0.046 (0.002)	78 (4)	0.053 (0.005)	52 (4)
7.52	0.002 (0.001)	12 (2)	0.003 (0.002)	4 (3)
	0.075 (0.003)	79 (3)	0.088 (0:005)	52 (4)
9.105	0.004 (0.003)	13 (2)	0.008 (0.004)	5 (3)
	0.108 (0.005)	78 (2)	0.126 (0.002)	53 (3)
11.79	0.010 (0.003)	14 (2)	0.020 (0.003)	6 (2)
	0.174 (0.005)	77 (2)	0.195 (0.003)	54 (3)

[a] Quantities in parentheses denote standard deviations. [b] In 10^{-6} s.

for translational diffusion by multiplying them by $\exp(-q^2Dt)$. From a computational standpoint, this procedure has several advantages over full simulations. First of all, noise is reduced since dynamic fluctuations due to translational diffusion are entirely eliminated. Second, total sampling time can be reduced over the low q range of interest since only faster rotational and, in the case of flexible structures, deformational motions contribute to the decay if $S(q,t)$. Finally, since uncorrected structure factors are simpler, their analysis and interpretation is more straightforward.

Summarized in Table V are the amplitudes and lifetimes extracted from uncorrected TDS normalized form factors ($S(q,t)/S(q,0)$) from rigid and flexible simulations. Although the amplitudes are comparable in both, the lifetimes are significantly shorter in the flexible case. This discrepancy persists, but at a reduced level, when corrected to include translational diffusion. This is summarized in Table VI. Also included here are experimental lifetimes and amplitudes from the work of Sorlie and Pecora.[18] Agreement between experiment and flexible model simulations is quite good if one chooses to ignore the very fast peak seen in the experiments. (This very fast peak could be due to afterpulsing.[26] Although similar short time peaks are frequently found in the simulations, their amplitudes are less than about 0.5% and are not reported.) The rigid model studies, on the other hand, yield first internal times that are consistently too long. Two conclusions can be drawn from this comparison. First, internal flexing and rotation contribute to τ_1. Second, the light-scattering experiments of 762 base pair DNA can best be explained by models that include segmental flexibility.

IV. Summary

In this work, an algorithm has been developed to simulate dynamics experiments of rigid macromolecules and has been applied to polarized dynamic light scattering.

Table VI
Comparison of Rigid and Flexible Model Studies with Experiments on 762 Base Pair DNA[a]

	rigid		flexible		expt[b]	
q^2, 10^{10} cm^{-2}	a	τ^c	a	τ^c	a	τ^c
4.171					0.03	7
	0.03 (0.02)	64 (12)	0.02 (0.01)	31 (10)	0.03	25
	0.97 (0.02)	272 (8)	0.98 (0.01)	262 (2)	0.94	263
5.895					0.05	5
	0.02 (0.01)	35 (3)	0.03 (0.01)	29 (3)	0.03	23
	0.98 (0.01)	184 (2)	0.97 (0.01)	184 (1)	0.92	180
7.52					0.06	4
	0.04 (0.01)	35 (2)	0.06 (0.01)	28 (3)	0.04	27
	0.96 (0.01)	143 (1)	0.94 (0.01)	144 (1)	0.90	142
9.105					0.08	4
	0.08 (0.01)	41 (3)	0.07 (0.01)	26 (2)	0.10	32
	0.92 (0.01)	118 (1)	0.93 (0.01)	116 (1)	0.82	124

[a] Quantities in parentheses denote standard deviations. [b] From ref 18. [c] In 10^{-6} s.

The algorithm has been tested and verified by examining a variety of rodlike structures in which the translational anisotropy is varied. Simulated first cumulants are in very good agreement with the theory of Wilcoxon and Schurr[11] while amplitudes and lifetimes are in very good agreement with the theories of Pecora[28] (isotropic case) and Aragon and Pecora[15] (anisotropic and isotropic cases). For 762 base pair DNA, it is concluded that translational anisotropy can be ignored, which makes it much more feasible to obtain simulated form factors with a high signal to noise ratio. In rigid and flexible model studies of this fragment, it is shown that segmental flexibility substantially reduces the first internal time and that models with flexibility are in much better agreement with experiment than models without flexibility.

Acknowledgment. I acknowledge the NSF for a Presidential Young Investigator Award and the donors of the Petroleum Research Fund, administered by the American Chemical Society, for partial support of this research. Dr. Susan Sorlie (Stanford University) and Professors Sergio Aragon (San Francisco State University) and Robert Pecora (Stanford University) also deserve special thanks.

Appendix

It is generally possible to uniquely determine the normalized column eigenvectors, $\mathbf{z}_i$, of a symmetric matrix, **D**, to within a sign of the eigenvectors.[24] In other words, the matrix

$$\mathbf{Z}' = \mathbf{ZK} \tag{A1}$$

where **Z** is given by eq 2

$$\mathbf{K} = \begin{pmatrix} (-)^a & 0 & 0 \\ 0 & (-)^b & 0 \\ 0 & 0 & (-)^c \end{pmatrix} \tag{A2}$$

and a, b, and c are each equal to 0 or 1 also diagonalize **D** following eq 1 in the text. Subscripts t and r shall be omitted for brevity.

Viewed another way, **D** can be diagonalized by carrying out a rotational transformation, **Q**, of the coordinate system from the lab frame to a principal axis (pa) frame in which **D** is diagonal[31]

$$\lambda = \mathbf{QDQ}^{\mathrm{T}} \tag{A3}$$

In comparing eq 1 with eq A3, it is tempting to equate **Q** and $\mathbf{Z}^{\mathrm{T}}$. However, the transformation **Z**, which is determined by diagonalization, could include an improper rotation or inversion. Consequently, we choose **K** such that

$$\mathbf{Q} = (\mathbf{Z}')^{\mathrm{T}} = \mathbf{KZ}^{\mathrm{T}} \tag{A4}$$

At the start of the simulation, we know **Z** (for both translation and rotation at time t_0) but not **K** and **Q**. However, **Q** can be calculated within the unknown factor **K**, which will turn out to be unimportant in the final analysis. Attention shall now be turned to the time evolution of **Q**.

If **p** is an arbitrary vector in reference frame Σ_a and **p**′ is the same vector in reference frame Σ_b, then

$$\mathbf{p}' = \mathbf{Q}(ab)\mathbf{p} \tag{A5}$$

where $\mathbf{Q}(ab)$ is the transformation matrix that carries Σ_a into Σ_b. This can be generalized in a straightforward way to treat multiple transformations

$$\mathbf{Q}(ac) = \mathbf{Q}(bc)\,\mathbf{Q}(ab) \tag{A6}$$

Σ_a denotes the lab frame and Σ_b, Σ_c, Σ_d, etc., denote pa frames at times t_0, $t_1 = t_0 + \delta t$, $t_2 = t_0 + 2\delta t$, etc. From eq A6 we can write

$$\mathbf{Q}(t_n) = \mathbf{U}(t_{n-1},\delta t)\,\mathbf{U}(t_{n-2},\delta t)\ldots\mathbf{U}(t_0,\delta t)\,\mathbf{Q}(t_0) \tag{A7}$$

where $\mathbf{Q}(t_n)$ carries the lab frame into the pa frame at time t_n and $\mathbf{U}(t_j,\delta t)$ is the rotation matrix, which carries the pa frame at time t_j into the new pa frame at time $t_j + \delta t$. Now **U** can be written in terms of rotation matrices where we first rotate about the x axis of the pa frame at time t_j by an amount ω_1, next rotate about the intermediate y axis by ω_2, and finally rotate about the intermediate z axis by ω_3. **U** can be written explicitly[31] as eq A8. For

$$\mathbf{U}(t_j\delta t) = \begin{pmatrix} \cos\omega_2\cos\omega_3 & \sin\omega_1\sin\omega_2\cos\omega_3 + \cos\omega_1\sin\omega_3 & -\cos\omega_1\sin\omega_2\cos\omega_3 + \sin\omega_1\sin\omega_3 \\ -\cos\omega_2\sin\omega_3 & -\sin\omega_1\sin\omega_2\sin\omega_3 + \cos\omega_1\cos\omega_3 & \cos\omega_1\sin\omega_2\sin\omega_3 + \sin\omega_1\cos\omega_3 \\ \sin\omega_2 & -\sin\omega_1\cos\omega_2 & \cos\omega_1\cos\omega_2 \end{pmatrix} \tag{A8}$$

rigid bodies and small δt, ω_1, ω_2, and ω_3 are determined by the rotational displacements about principal axes 1–3 between t_j and $t_j + \delta t$, respectively. In Brownian dynamics they are given by

$$\omega_i = (\lambda_{ri})^{1/2} x_i \tag{A9}$$

where λ_{ri} is the ith eigenvalue of $\mathbf{D}_r$ and x_i is a gaussian random number of zero mean and variance $(2\delta t)^{1/2}$. For small δt and consequently small ω_i, eq A8 becomes

$$\mathbf{U}(t_j,\delta t) = \begin{pmatrix} 1 & \omega_3 & -\omega_2 \\ -\omega_3 & 1 & \omega_1 \\ \omega_2 & -\omega_1 & 1 \end{pmatrix} \tag{A10}$$

Attention shall now be turned to the time evolution of $\mathbf{s}_i$.

From eq A5 we can write

$$\mathbf{s}_i^{\text{par}} = \mathbf{Q}_r(t_n)\, \mathbf{s}_i(t_n) \tag{A11}$$

where $\mathbf{s}_i^{\text{par}}$ is the relative position vector of subunit i in the principal axis of rotation reference frame. For a rigid body, $\mathbf{s}_i^{\text{par}}$ will be time invariant. Combining eq A4 with eq A11 at t_0

$$\mathbf{s}_i^{\text{par}} = \mathbf{K}_r \mathbf{Z}_r^{\mathrm{T}}(t_0)\, \mathbf{s}_i(t_0) \tag{A12}$$

Inverting eq A11 and using eqs A7 and A4

$$\begin{aligned} \mathbf{s}_i(t_n) &= \mathbf{Q}_r^{\mathrm{T}}(t_n)\, \mathbf{s}_i^{\text{par}} \\ &= \mathbf{Q}_r^{\mathrm{T}}(t_0)\, \mathbf{P}(t_0,t_n)\, \mathbf{K}_r \mathbf{Z}_r^{\mathrm{T}}(t_0)\, \mathbf{s}_i(t_0) \\ &= \mathbf{Z}_r(t_0)\, [\mathbf{K}_r \mathbf{P}(t_0,t_n) \mathbf{K}_r] \mathbf{Z}_r^{\mathrm{T}}(t_0)\, \mathbf{s}_i(t_0) \end{aligned} \tag{A13}$$

where

$$\mathbf{P}(t_0,t_n) = \mathbf{U}^{\mathrm{T}}(t_0,\delta t)\, \mathbf{U}^{\mathrm{T}}(t_1,\delta t) \ldots \mathbf{U}^{\mathrm{T}}(t_{n-1},\delta t) \tag{A14}$$

Since $\mathbf{K}_r \mathbf{K}_r = \mathbf{I}$ ($\mathbf{I}$ is the 3×3 identity matrix), it can be sandwiched between each of the $\mathbf{U}^{\mathrm{T}}$ terms in eq A14. Consequently, the quantity in brackets in eq A13 can be written as a matrix product of n-independent $\mathbf{K}_r \mathbf{U}^{\mathrm{T}} \mathbf{K}_r$ matrices. From eq A2

$$(\mathbf{K}r\mathbf{U}^{\mathrm{T}}\mathbf{K}^r)_{ij} = (\mathbf{K}_r)_{ii} (\mathbf{K}_r)_{jj} U_{ji} \tag{A15}$$

$\mathbf{K}_r$ will have no effect on the diagonal terms, and for small displacements, where eq A10 holds, the off-diagonal terms may change sign. However, since the off-diagonal terms are proportional to the randomly generated ω_i, which are as likely to be positive as negative, $\mathbf{K}_r$ will have no average effect on the time evolution of the structure. Hence, we can ignore $\mathbf{K}_r$ altogether, which yields eq 5 in the text.

Finally, the time evolution of the center of diffusion is considered. Let

$$\mathbf{r}_{CD}(t_{n+1}) = \mathbf{r}_{CD}(t_n) + \delta \mathbf{r}_{CD}(t_n) \tag{A16}$$

In the principle axis of translation (pat) frame, the displacement of the center of diffusion is diagonal

$$\delta \mathbf{r}_{CD}^{\text{pat}}(t_n) = \lambda_t^{1/2} \mathbf{x}_{CD} \tag{A17}$$

where $\lambda_t^{1/2}$ is a diagonal 3×3 matrix with elements equal to the square root of the elements of λ_t and $\mathbf{x}_{CD}$ is a vector of independent Gaussian random numbers of 0 mean and variance $(2\ \delta t)^{1/2}$. From eq A5 we can write

$$\begin{aligned} \delta \mathbf{r}_{CD}(t_n) &= \mathbf{Q}_t^{\mathrm{T}}(t_n)\, \delta \mathbf{r}_{CD}^{\text{pat}}(t_n) \\ &= \mathbf{Q}_t^{\mathrm{T}}(t_n)\, \lambda_t^{1/2} \mathbf{x}_{CD} \end{aligned} \tag{A18}$$

If the structure only translated, there would be no change in $\mathbf{Q}_t$ with time. However, because of rotation, $\mathbf{Q}_t$ changes. Use eq A6 and let Σ_a denote the lab frame, and Σ_b/Σ_c, the par/pat frame at t_n. Then

$$\mathbf{Q}_t(t_n) = \mathbf{Q}_{rp} \mathbf{Q}_r(t_n) \tag{A19}$$

where $\mathbf{Q}_{rp}$ transforms from the par to pat reference frames. $\mathbf{Q}_{rp}$ will be time independent. Setting $t_n = t_0$ in eq A19, post-multiplying both sides by $\mathbf{Q}_r^{\mathrm{T}}(t_0)$, and taking the transpose yields

$$\mathbf{Q}_{rp}^{\mathrm{T}} = \mathbf{K}_r \mathbf{Z}_r^{\mathrm{T}}(t_0)\, \mathbf{Z}_t(t_0)\, \mathbf{K}_t \tag{A20}$$

After several straightforward substitutions

$$\delta \mathbf{r}_{CD}(t_n) = \mathbf{Z}_r(t_0) [\mathbf{K}_r \mathbf{P}(t_0,t_n)\, \mathbf{K}_r] \mathbf{Z}_r^{\mathrm{T}}(t_0)\, \mathbf{Z}_t(t_0)\, \mathbf{K}_t\, \lambda_t^{1/2} \mathbf{x}_{CD} \tag{A21}$$

For the same reason as before, the $\mathbf{K}_r$'s can be ignored. Similarly $\mathbf{K}_t$ can be absorbed by the Gaussian random number vector, $\mathbf{x}_{CD}$. Without loss of generality, the $\mathbf{K}$ matrices in eq A21 can be ignored, which yields eq 9 in the text.

References and Notes

(1) Belford, G. G.; Belford, R. L.; Weber, G. *Proc. Natl. Acad. Sci. U.S.A.* **1972**, *69*, 1392.
(2) Ehrenberg, M.; Rigler, R. *Chem. Phys. Lett.* **1972**, *14*, 539.
(3) Wegener, W. A.; Dowben, R. M.; Koester, V. J. *J. Chem. Phys.* **1979**, *70*, 622.
(4) Aragon, S. R.; Pecora, R. *J. Chem. Phys.* **1977**, *66*, 2506.
(5) Schaefer, D. W.; Benedek, G. B.; Schofield, P.; Bradford, E. *J. Chem. Phys.* **1971**, *55*, 3884.
(6) Fraser, A. B.; Eisenberg, E.; Kielley, W. W.; Carlson, F. D. *Biochemistry* **1975**, *14*, 2207.
(7) Newman, J.; Carlson, F. D. *Biophys. J.* **1980**, *29*, 37.
(8) Maeda, H.; Saito, N. *J. Phys. Soc. Jpn.* **1969**, *27*, 984.
(9) Maeda, H.; Saito, N. *Polym. J.* **1973**, *4*, 309.
(10) Rallison, J. M.; Leal, L. G. *J. Chem. Phys.* **1981**, *74*, 4819.
(11) Wilcoxon, J.; Schurr, J. M. *Biopolymers* **1983**, *22*, 849.
(12) Aragon, S. R. In *Surfactants in Solution*; Mittal, K. L., Ed.; Plenum: New York, 1989; Vol. 7, p 105.
(13) Maeda, T.; Fujime, S. *Macromolecules* **1984**, *17*, 1157.
(14) Kubota, K.; Urabe, H.; Tominga, Y.; Fujime, S. *Macromolecules* **1984**, *17*, 2096.
(15) Aragon, S. R.; Pecora, R. *J. Chem. Phys.* **1985**, *82*, 5346.
(16) Koppel, D. E. *J. Chem. Phys.* **1972**, *57*, 4814.
(17) Provencher, S. W. *Comput. Phys. Commun.* **1982**, *27*, 213, 229.
(18) Sorlie, S. S.; Pecora, R. *Macromolecules* **1990**, *23*, 487.
(19) Allison, S. A. *Macromolecules* **1986**, *19*, 118.
(20) Allison, S. A.; Sorlie, S. S.; Pecora, R. *Macromolecules* **1990**, *23*, 1110.
(21) Garcia de la Torre, J.; Bloomfield, V. A. *Q. Rev. Biophys.* **1981**, *14*, 81.
(22) Hagerman, P. J.; Zimm, B. H. *Biopolymers* **1981**, *20*, 1481.
(23) Garcia de la Torre, J.; Jiminez, A.; Freire, J. J. *Macromolecules* **1982**, *15*, 148.
(24) IMSL Library 9.2 Reference Manual, IMSL International and Statistical Libraries, Inc., Houston, TX, 1986.
(25) Berne, B. J.; Pecora, R. In *Dynamic Light Scattering*; Wiley: New York, 1976.
(26) Sorlie, S. S.; Pecora, R. **1988**, *21*, 1437.
(27) Rotne, J.; Prager, S. *J. Chem. Phys.* **1969**, *50*, 4831.
(28) Pecora, R. *J. Chem. Phys.* **1964**, *40*, 1604.
(29) Schurr, J. M.; Allison, S. A. *Biopolymers* **1981**, *20*, 251.
(30) Lewis, R. J.; Allison, S. A.; Eden, D.; Pecora, R. *J. Chem. Phys.* **1988**, *89*, 2490.
(31) Arfken, G. In *Mathematical Methods for Physicists*; Academic Press: New York, 1970; Chapter 4.